LETTERS

# The type IV mucolipidosis-associated protein TRPML1 is an endolysosomal iron release channel

Xian-Ping Dong[1], Xiping Cheng[1], Eric Mills[1], Markus Delling[2], Fudi Wang[3], Tino Kurz[4] & Haoxing Xu[1]

**TRPML1 (mucolipin 1, also known as MCOLN1) is predicted to be an intracellular late endosomal and lysosomal ion channel protein that belongs to the mucolipin subfamily of transient receptor potential (TRP) proteins[1–3]. Mutations in the human *TRPML1* gene cause mucolipidosis type IV disease (ML4)[4,5]. ML4 patients have motor impairment, mental retardation, retinal degeneration and iron-deficiency anaemia. Because aberrant iron metabolism may cause neural and retinal degeneration[6,7], it may be a primary cause of ML4 phenotypes. In most mammalian cells, release of iron from endosomes and lysosomes after iron uptake by endocytosis of $Fe^{3+}$-bound transferrin receptors[6], or after lysosomal degradation of ferritin–iron complexes and autophagic ingestion of iron-containing macromolecules[6,8], is the chief source of cellular iron. The divalent metal transporter protein DMT1 (also known as SLC11A2) is the only endosomal $Fe^{2+}$ transporter known at present and it is highly expressed in erythroid precursors[6,9]. Genetic studies, however, suggest the existence of a DMT1-independent endosomal and lysosomal $Fe^{2+}$ transport protein[9]. By measuring radiolabelled iron uptake, by monitoring the levels of cytosolic and intralysosomal iron and by directly patch-clamping the late endosomal and lysosomal membrane, here we show that TRPML1 functions as a $Fe^{2+}$ permeable channel in late endosomes and lysosomes. ML4 mutations are shown to impair the ability of TRPML1 to permeate $Fe^{2+}$ at varying degrees, which correlate well with the disease severity. A comparison of *TRPML1*$^{-/-}$ ML4 and control human skin fibroblasts showed a reduction in cytosolic $Fe^{2+}$ levels, an increase in intralysosomal $Fe^{2+}$ levels and an accumulation of lipofuscin-like molecules in *TRPML1*$^{-/-}$ cells. We propose that TRPML1 mediates a mechanism by which $Fe^{2+}$ is released from late endosomes and lysosomes. Our results indicate that impaired iron transport may contribute to both haematological and degenerative symptoms of ML4 patients.**

Release of $Fe^{2+}$ from late endosomes and lysosomes into the cytosol is essential for cellular iron metabolism (see Supplementary Fig. 1)[6]. Because TRPML1 is ubiquitously expressed (in cells of every tissue)[5] and primarily localized in the late endosome and lysosome (LEL)[1,3,10], we propose that TRPML1 may act as an endolysosomal $Fe^{2+}$ release channel. The intracellular localization of wild-type TRPML1 (refs 1, 3 and 10; see also Supplementary Fig. 2), however, makes it difficult to assay the function of this channel. To overcome this problem, we recently developed a functional assay for TRPML channels[11]. A spontaneous mouse mutation (A419P)[12] markedly increases TRPML3-mediated currents at the plasma membrane without altering its permeation properties[11]. Mice carrying this mutation (varitint-waddler, *Va*) are deaf and show skin pigmentation defects. When the *Va* mutation (proline substitution) was introduced into a homologous position in TRPML1 (V432P), the mutant channel TRPML1$^{Va}$ was (mis)localized in many cellular compartments including both LEL and the plasma membrane (Supplementary Fig. 2). Notably, TRPML1$^{Va}$, but not wild-type TRPML1, generated a cationic whole-cell current that can be measured by patch clamp[11].

We studied TRPML proteins by transiently expressing them in HEK293T cell lines. To monitor expression, TRPML channels were fused to enhanced green fluorescent protein (EGFP) at their amino termini. In response to a voltage step protocol, TRPML1$^{Va}$-expressing cells showed strong inwardly rectifying step currents (Fig. 1a and Supplementary Fig. 3) in a standard extracellular bath solution (a modified Tyrode's solution). TRPML1$^{Va}$-mediated current ($I_{TRPML1^{Va}}$) was $101 \pm 8.6$ pA pF$^{-1}$ at $-80$ mV (mean $\pm$ s.e.m., $n = 48$). To mimic the acidic environments of lysosomes where the extracellular side (analogous to the intralysosomal luminal side) of the wild-type TRPML1 protein is exposed to, extracellular solutions were adjusted to pH 4.6. No sizable inward current was detected when *N*-methyl-D-glucamine ($NMDG^+$) was the only major cation in the bath (pH 4.6; Fig. 1b), indicating that $I_{TRPML1^{Va}}$ is a proton-impermeable cationic current[11]. Bath perfusion of 30 mM extracellular $[Fe^{2+}]$ ($[Fe^{2+}]_o$, pH 4.6) to TRPML1$^{Va}$-expressing cells induced large inwardly rectifying currents (Fig. 1c). The current density of $[Fe^{2+}]_o$-elicited $I_{TRPML1^{Va}}$ ($I_{Fe/TRPML1^{Va}}$) at $-80$ mV was $74 \pm 8.6$ pA pF$^{-1}$ (mean $\pm$ s.e.m., $n = 24$). To keep $Fe^{2+}$ in a reduced state, ascorbic acid was used as the counter anion in the bath solution. The only other main cation in the 30 mM $Fe^{2+}$ solution was $NMDG^+$. Thus, $I_{Fe/TRPML1^{Va}}$ is carried solely by $Fe^{2+}$. Consistent with this, the amplitude of $I_{Fe/TRPML1^{Va}}$ was strongly dependent on $[Fe^{2+}]_o$ (Supplementary Fig. 4).

Both $I_{Fe/TRPML1^{Va}}$ (Fig. 1e) and $I_{TRPML1^{Va}}$[11] were enhanced at low pH. Compared to experiments conducted at physiological pH (7.4), $I_{Fe/TRPML1^{Va}}$ was enhanced $\sim$2-fold at pH 4.6 (approximately the luminal pH of lysosomes). In cells transfected with TRPML2$^{Va}$ (a short splice variant; see Methods), a large current ($23.0 \pm 3.8$ pA pF$^{-1}$ at $-80$ mV, $n = 7$) was evoked by 30 mM $Fe^{2+}$ (pH 4.6, Fig. 1e). Similar to $I_{TRPML1^{Va}}$, $I_{TRPML2^{Va}}$ was also strongly potentiated by low pH (Supplementary Fig. 5). The ratio of $I_{Fe}/I_{Tyrode}$ for TRPML2$^{Va}$ was $139 \pm 22\%$ (at $-80$ mV, $n = 7$), which was even larger than the ratio for TRPML1$^{Va}$ ($72 \pm 7\%$, $n = 11$). In contrast with TRPML1$^{Va}$ and TRPML2$^{Va}$, the ratio of $I_{Fe}/I_{Tyrode}$ for TRPML3$^{Va}$ was only $2.3 \pm 0.2\%$ ($n = 8$; Fig. 1f). Thus, $Fe^{2+}$ permeability is specific for TRPML1 and TRPML2, but not for the closely related TRPML3. Cationic selectivity analysis suggested that TRPML1$^{Va}$ was also permeable to most other divalent trace metals including $Mn^{2+}$ and $Zn^{2+}$, but not to $Fe^{3+}$ (Supplementary Fig. 6). Detailed analyses of the permeation properties of TRPML1$^{Va}$ suggested that the conduction mechanism of $Fe^{2+}$ resembled those of $Na^+$ and $Ca^{2+}$ (see Supplementary Figs 7–9).

[1]The Department of Molecular, Cellular, and Developmental Biology, The University of Michigan, 3089 Natural Science Building (Kraus), 830 North University, Ann Arbor, Michigan 48109, USA. [2]The Department of Cardiology, Children's Hospital Boston, Enders 1350, 320 Longwood Avenue, Boston, Massachusetts 02115, USA. [3]Institute for Nutritional Sciences, Shanghai Institutes for Biological Sciences, Chinese Academy of Sciences, Shanghai 200031, China. [4]Department of Pharmacology, Faculty of Health Science, University of Linköping, S-58185 Linköping, Sweden.

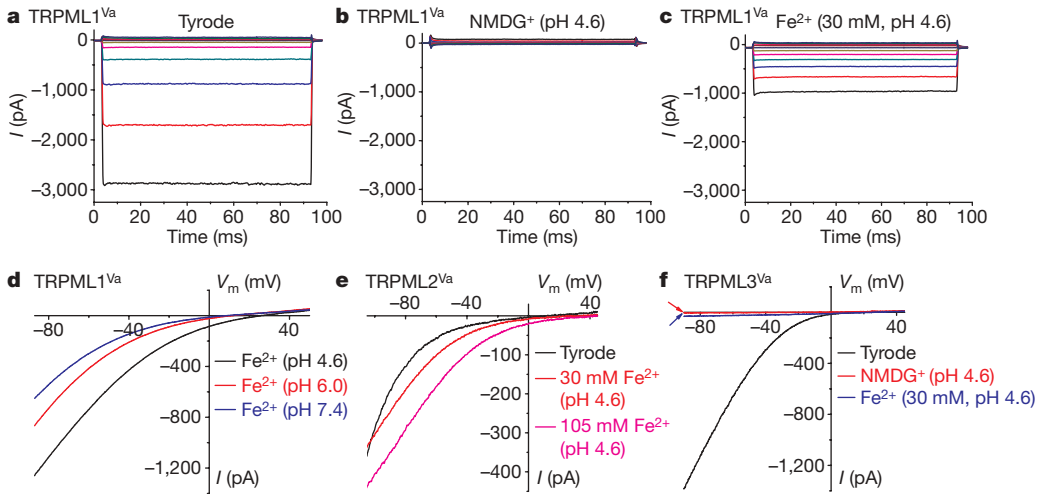


**Figure 1 | TRPML1$^{Va}$-expressing cells have a constitutively active H$^+$-modulated Fe$^{2+}$ current.** **a**, A TRPML1$^{Va}$-expressing HEK293T cell showed a large inwardly rectifying whole-cell current elicited by voltage steps (from −140 mV to +80 mV in increments of 20 mV) in the standard extracellular (Tyrode's) bath solution. Step duration, 90 ms; holding potential, 0 mV; $V_m$, membrane potential. **b**, No significant inward current was detected in NMDG$^+$ ($Na^+$-free, $Ca^{2+}$-free, pH 4.6) solution. **c**, Inwardly rectifying step currents were evoked by 30 mM $Fe^{2+}$ solution (pH 4.6) in the same cell as shown in **a** and **b**. **d**, pH-dependence of $I_{Fe/TRPML1^{Va}}$. Whole-cell currents were elicited by repeated voltage ramps (−100 to +100 mV; 400 ms) with a 4-s interval between ramps. Only a portion of the voltage protocol is shown. Holding potential, 0 mV. **e**, Large $I_{Fe/TRPML2^{Va}}$ was seen in the presence of 30 and 105 mM $Fe^{2+}$ (pH 4.6). **f**, Little or no $I_{Fe}$ was seen in a TRPML3$^{Va}$-expressing cell.

Next, we tested whether the $Fe^{2+}$ permeability of TRPML1 is impaired by ML4 mutations. More than 15 ML4 mutations have been identified, most of which are located in the transmembrane regions of TRPML1 (Supplementary Fig. 10)[4,5,13,14]. We constructed six of these ML4 mutants into the TRPML1$^{Va}$ background and investigated the $Fe^{2+}$ permeability of these combined mutations. We found that all ML4 mutant TRPML1$^{Va}$ channels had significantly smaller $I_{Fe}$ than TRPML1$^{Va}$. In particular, T232P, D362Y and V446L mutations (combined with the *Va* mutation) completely eliminated $I_{Fe}$, as well as $I_{Tyrode}$ (Fig. 2a and Supplementary Fig. 11), although the protein expression levels and subcellular localization pattern of these mutants were similar to those of the parental TRPML1$^{Va}$ protein (Supplementary Figs 12 and 13). Patients carrying these mutations are reported to have severe phenotypes[5,15]. On the other hand, a large $I_{Fe}$ was detected in F408Δ-TRPML1$^{Va}$-transfected cells. The average current density of this mutant, however, was still significantly smaller than $I_{Fe/TRPML1^{Va}}$. Patients carrying the F408Δ mutation have unusually mild phenotypes[13,15]. Small but evident $I_{Fe}$ was detected with expression of two other mutants (R403C and F465L). A patient carrying the R403C mutation was reported to have a relatively mild phenotype[14]. Taken together, these results

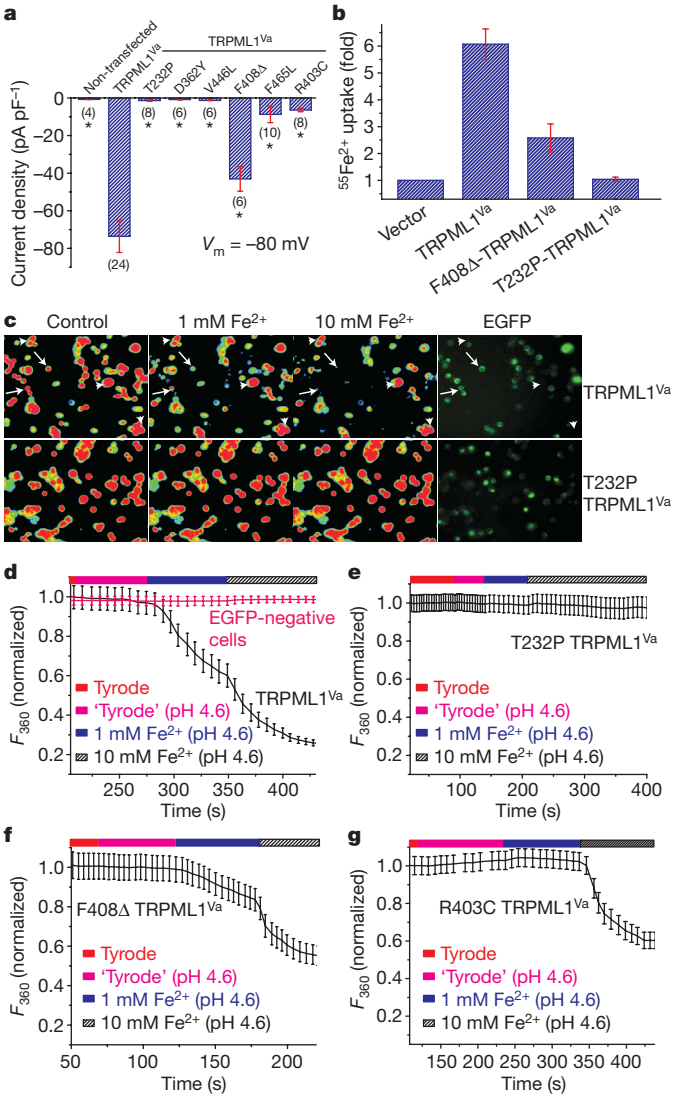


**Figure 2 | Fe$^{2+}$ permeability of the TRPML1 channel is impaired by ML4 mutations.** **a**, Current densities (mean ± s.e.m., $n$ = 4–10) of $I_{Fe}$ (30 mM $Fe^{2+}$, pH 4.6) for TRPML1$^{Va}$ and ML4 mutant TRPML1$^{Va}$ channels. Asterisk indicates statistical difference ($P < 0.01$) compared to TRPML1$^{Va}$. **b**, $^{55}Fe^{2+}$ uptake (normalized) in HEK293T cells transfected with vector control, with TRPML1$^{Va}$, with F408Δ-TRPML1$^{Va}$ and with T232P-TRPML1$^{Va}$ constructs. Error bars indicate the standard deviation on the basis of two independent triplicate experiments. **c**, $[Fe^{2+}]_o$-dependent quenching of Fura-2 fluorescence in TRPML1$^{Va}$-transfected cells (arrows), but not in non-transfected control cells (arrowheads) or T232P-TRPML1$^{Va}$-transfected cells (bottom row). The fluorescence intensity was measured at an excitation wavelength of 360 nm ($F_{360}$). The original magnification used for all micrographs was ×200. **d**, Average normalized responses of EGFP-positive TRPML1$^{Va}$-transfected cells (typically $n$ = 20–40 cells) to 1 or 10 mM $Fe^{2+}$ (pH 4.6). **e**, No significant quenching was seen in T232P-TRPML1$^{Va}$-transfected cells. **f**, Slightly less quenching was observed for the F408Δ-TRPML1$^{Va}$-expressing cells. **g**, A small but significant quenching reaction was detected (with 10 mM $Fe^{2+}$) in R403C-TRPML1$^{Va}$-expressing cells.

indicate that ML4 mutations significantly impair the $Fe^{2+}$ permeability of TRPML1. The degree of the impaired $Fe^{2+}$ permeability seems to correlate well with disease severity observed in ML4 patients.

To investigate $TRPML1^{Va}$-mediated $Fe^{2+}$ influx under less invasive conditions in intact cells, we measured $^{55}Fe^{2+}$ uptake at low pH (pH 5.8, 1 μM $^{55}Fe^{2+}$; Fig. 2b). Significant $^{55}Fe^{2+}$ uptake was seen in HEK293T cells transfected with $TRPML1^{Va}$, but not with T232P-$TRPML1^{Va}$. An intermediate $^{55}Fe^{2+}$ uptake was seen for F408Δ-$TRPML1^{Va}$. These results indicate that $TRPML1^{Va}$ can mediate significant $Fe^{2+}$ entry even at micromolar $[Fe^{2+}]_o$. We also adopted a fluorescence-based $Fe^{2+}$ quenching assay to measure $TRPML1^{Va}$-mediated $Fe^{2+}$ entry in HEK293T cells. Heavy metals such as $Mn^{2+}$ and $Fe^{2+}$ can bind $Ca^{2+}$-sensitive dyes such as Fura-2 with higher affinity, resulting in strong fluorescence quenching effects[16]. Substantial quenching of Fura-2 fluorescence was seen in $TRPML1^{Va}$-expressing cells after the addition of 1 mM $Fe^{2+}$ (pH 4.6; Fig. 2d, f). Increased quenching was observed with the addition of higher concentrations of $Fe^{2+}$ (10 mM, pH 4.6). In contrast, no significant quenching was detected in neighbouring non-transfected EGFP-negative cells or $TRPML3^{Va}$-transfected cells (1 mM $Fe^{2+}$; Supplementary Fig. 14). ML4 mutant $TRPML1^{Va}$-expressing HEK293T cells showed an impairment of $Fe^{2+}$ quenching. No significant $Fe^{2+}$ quenching was seen in T232P- (Fig. 2e), D362Y-, or V446L-$TRPML1^{Va}$-expressing cells (data not shown). Slightly less quenching was observed for F408Δ-$TRPML1^{Va}$ (Fig. 2f). In contrast, R403C-$TRPML1^{Va}$ (Fig. 2g) and F465L-$TRPML1^{Va}$ showed no response to the addition of 1 mM $Fe^{2+}$. However, a higher concentration of $Fe^{2+}$ (10 mM) induced a slow but significant quenching. These results agree with the electrophysiological measurements of ML4 mutants, as well as the disease severity of ML4 patients carrying

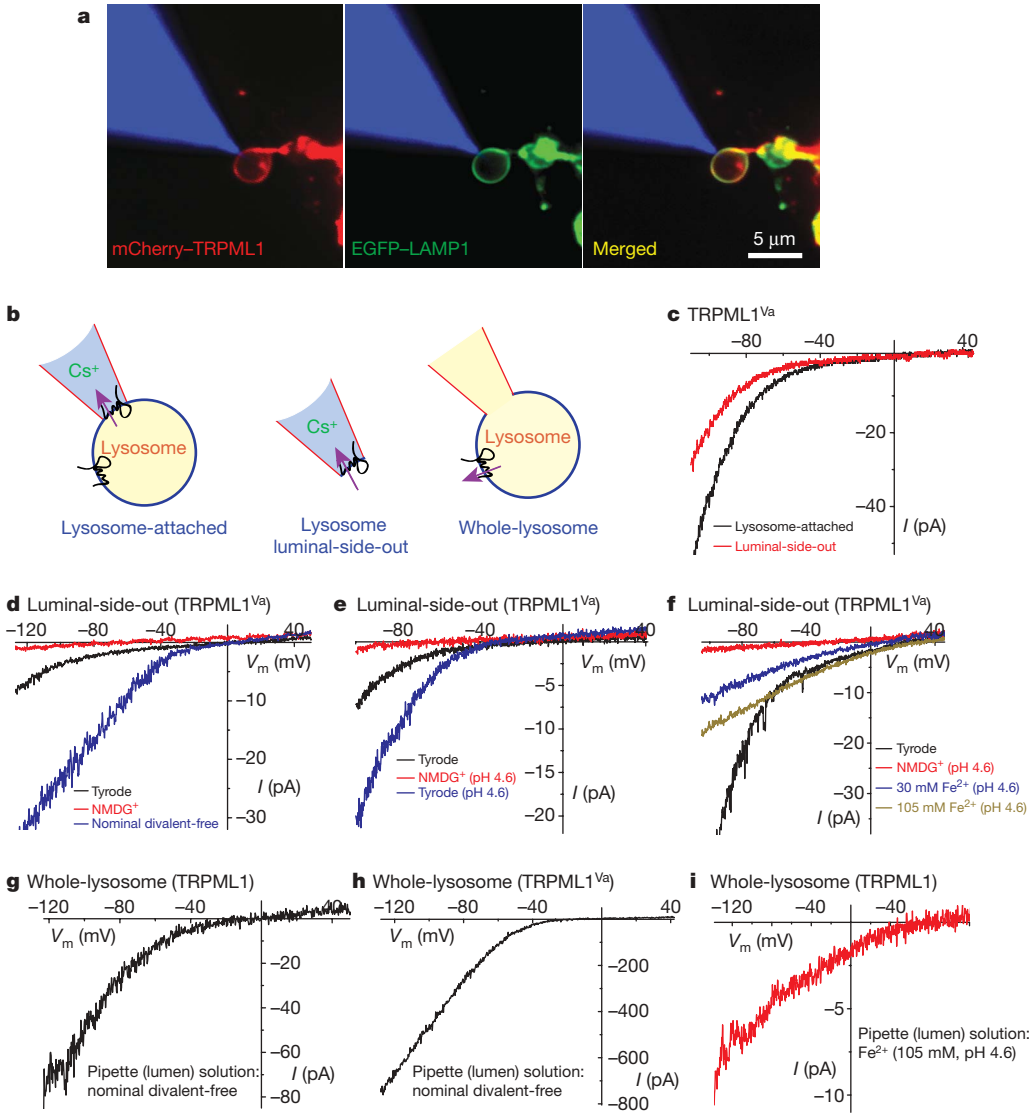


**Figure 3 | TRPML1 conducts $Fe^{2+}$ in late endosomes and lysosomes.** **a**, Co-localization of mCherry–TRPML1 and EGFP–LAMP1 at the membrane of an isolated enlarged LEL (see Methods). The patch pipette was filled with red rhodamine B dye (shown in blue for the purpose of illustration). **b**, Cartoons of three distinct patch-clamp configurations of lysosomal recordings: lysosome-attached, lysosome luminal-side-out and whole-lysosome. In each configuration, the pink arrow indicates the direction of the inward (at negative potentials; flow out of the lysosomes) current mediated by TRPML1 (as shown in **c**–**i**). **c**, Lysosomal $I_{TRPML1^{Va}}$. Switching from lysosome-attached to (lysosome) luminal-side-out configuration significantly reduced the amplitude of the current. The luminal-side-out patch was exposed to the Tyrode's solution. A $Cs^+$-based solution (147 mM Cs-methanesulphonate (Cs-MSA)) was used as a pipette solution for both configurations. **d**, $NMDG^+$-impermeable lysosomal $I_{TRPML1^{Va}}$ was much larger in the absence of divalent cations (nominal divalent-free). **e**, Lowering pH potentiated lysosomal $I_{TRPML1^{Va}}$. **f**, $I_{Fe/TRPML1^{Va}}$ induced by 30 mM and 105 mM $Fe^{2+}$. **g**, Whole-lysosome current in an enlarged lysosome expressing wild-type TRPML1. The pipette (lumen) solution contained nominal divalent-free Tyrode solution. A $Cs^+$-based bath solution (147 mM Cs-MSA) was used. **h**, Whole-lysosome $I_{TRPML1^{Va}}$. **i**, Whole-lysosome $I_{Fe/TRPML1}$. The pipette (lumen) solution contained 105 mM $Fe^{2+}$ (pH 4.6).

these mutations[5,13–15]. Thus, ML4 phenotypes result from a loss-of-function of TRPML1 with respect to $Fe^{2+}$ and/or $Ca^{2+}$ permeability.

To validate our use of $TRPML1^{Va}$ as a model to extrapolate potential intracellular functions of wild-type TRPML1, and more importantly, to confirm whether wild-type TRPML1 conducts $Fe^{2+}$ from the lumen of LEL into the cytosol, we performed patch-clamp recordings directly on native LEL membranes (Fig. 3a and Supplementary Fig. 15; see Methods). In $TRPML1^{Va}$-positive enlarged LEL, large inwardly rectifying currents were seen under the lysosome-attached configuration (Fig. 3b, c). The currents became smaller when the patch was excised (lysosome luminal-side-out) and exposed to Tyrode's solution (Fig. 3c). These large inwardly rectifying currents were not seen in $TRPML1^{Va}$-negative vacuoles, suggesting that these lysosomal currents are mediated by $TRPML1^{Va}$ (hereafter referred to as lysosomal $I_{TRPML1^{Va}}$). Note that inward lysosomal currents are actually currents that flow out of the lysosomes. Similar to $I_{TRPML1^{Va}}$ recorded at the plasma membrane, lysosomal $I_{TRPML1^{Va}}$ was impermeable to $NMDG^+$ and $H^+$, but was potentiated by low pH or by removal of divalent cations in the bath solution (nominal divalent-free; Fig. 3d, e). When the luminal-side-out patches were exposed to 30 mM or 105 mM $Fe^{2+}$ solutions (pH 4.6), smaller and less rectifying currents were seen, resembling $I_{Fe/TRPML1^{Va}}$ at the plasma membrane. These results indicate that $TRPML1^{Va}$ behaves similarly at both plasma and lysosomal membranes. Likewise, ML4 mutant $TRPML1^{Va}$ channels also behaved similarly as their plasma membrane counterparts (Supplementary Fig. 16), consistent with our conclusion that ML4 mutations primarily affect the channel function of TRPML1.

Next we performed whole-lysosome recordings on enlarged LEL expressing wild-type TRPML1 and $TRPML1^{Va}$. Significant inwardly rectifying currents were seen in wild-type TRPML1-positive LEL ($81.0 \pm 9.0$ pA $pF^{-1}$ at $-120$ mV, $n = 6$; Fig. 3g) with nominal divalent-free solution in the luminal side (that is, pipette solution), although the current amplitude is still one order of magnitude smaller than the whole-lysosome current recorded from $TRPML1^{Va}$-positive LEL ($1{,}713 \pm 404$ pA $pF^{-1}$ at $-120$ mV, $n = 4$; Fig. 3h). Because we were not able to record any significant whole-cell current from wild-type TRPML1-expressing HEK293T cells[11], our results indicate that the *Va* mutation affects both channel gating and trafficking (between LEL and the plasma membrane) of TRPML1. When isotonic (105 mM) $Fe^{2+}$ solution was included in the luminal side of wild-type TRPML1-positive enlarged LEL, inwardly rectifying currents with very positive reversal potential were observed ($18 \pm 4$ pA $pF^{-1}$ at $-120$ mV, $n = 4$; Fig. 3i). Collectively, these results indicate that wild-type TRPML1 is a lysosomal $Fe^{2+}$-permeable channel, and that the *Va* mutation does not alter the permeation properties of the TRPML1 channel.

Retention of $Fe^{2+}$ in LEL due to loss or inactivation of the $Fe^{2+}$ release mechanism may result in an insufficient supply of cytosolic $Fe^{2+}$. We therefore measured the levels of free (chelatable) intracellular $Fe^{2+}$ in skin fibroblasts from a ML4 patient ($TRPML1^{-/-}$) and the non-diseased parent ($TRPML1^{+/-}$) using a fluorescence-based iron de-quenching imaging method (see Methods)[17]. Chelatable $Fe^{2+}$ levels were significantly lower in $TRPML1^{-/-}$ cells compared to the control $TRPML1^{+/-}$ cells (Fig. 4a, b). TRPML1-deficient skin fibroblast cells show autofluorescence (Fig. 4c) at excitation wavelengths between 440 nm and 500 nm, reminiscent of accumulated lipofuscin-like substances previously reported[18]. The autofluorescence observed was primarily localized in LAMP1 (a marker for LEL)-positive compartments (Fig. 4c), indicative of a lysosomal dysfunction in $TRPML1^{-/-}$ cells. Lipofuscin, also referred to as an 'ageing pigment', is a non-degradable oxidized polymeric substance containing proteins, lipids, carbohydrates and iron[19]. The production of lipofuscin is facilitated by increased intralysosomal $Fe^{2+}$ levels[19]. Our results indicate that an accumulation of autofluorescent lipofuscin-like molecules in $TRPML1^{-/-}$ cells might result from impaired intralysosomal iron metabolism. Consistent with this, lysosomal iron staining experiments showed that $TRPML1^{-/-}$ cells had higher lysosomal iron content than control cells (Supplementary Fig. 17).

We have demonstrated that TRPML1 has a critical role in cellular iron homeostasis by showing the cytosolic $Fe^{2+}$ deficiency with concurrent intralysosomal iron overload in ML4 cells. ML4 cells show a defect in the late endocytic pathway[10,20,21], suggesting that TRPML1 may be required for $Ca^{2+}$-dependent fusion or fission of LEL. However, this defect in vesicular transport cannot explain the cytosolic $Fe^{2+}$ deficiency that we observed because the internalization and recycling of the transferrin receptor is normal in ML4 cells[20], and lysosomal $Fe^{2+}$ release (into the cytosol) is probably mediated directly by an iron-conducting channel/transporter, as is the case for DMT1 (ref. 22). Therefore, by far the simplest explanation of our results is that the $Fe^{2+}$ release pathway between the cytosol and the lysosome lumen is blocked or inactivated in cells with ML4 mutations. Although a ML4-induced loss of $Ca^{2+}$ permeability may result in a defect in lysosomal trafficking and subsequent accumulation of various lipids in LEL, the degradation of these materials is normal[20,21]. Therefore, these accumulated substances would become most harmful only if they are oxidized to generate lipofuscin-like non-degradable materials in the presence of high intralysosomal $Fe^{2+}$ (ref. 19). Lipofuscin-like molecules preferentially accumulate in post-mitotic cells such as muscle cells and neurons, which are primarily affected in ML4 patients[21]. Our work suggests that lysosome-targeting iron chelators might alleviate the degenerative symptoms of ML4 patients.

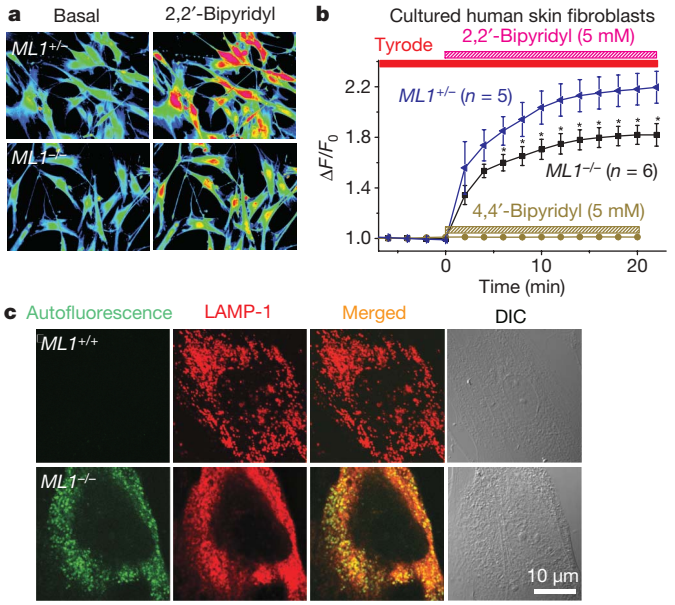


**Figure 4 | TRPML1-deficient cells have reduced free (chelatable) iron levels and lysosomal autofluorescence. a**, Cultured $TRPML1^{-/-}$ ($ML1^{-/-}$) skin fibroblasts showed less de-quenching of the iron-sensitive fluorescence than $ML1^{+/-}$ cells did. De-quenching was achieved by preloading the fibroblasts with an iron-sensitive dye, Phen Green SK (PG SK), and then adding the membrane-permeable transition metal chelator, 2,2′-bipyridyl (BPD). 2,2′-BPD is predicted to chelate free cellular iron (also referred to as chelatable or labile iron), which subsequently increases PG SK fluorescence. The original magnification used was ×200. **b**, The average 2,2′-BPD induced normalized change of fluorescence ($\Delta F/F_0$) for ML4 cells ($ML1^{-/-}$; $n = 6$ experiments) is significantly (asterisk, $P < 0.01$) lower than for the parental $ML1^{+/-}$ cells. Fibroblast cells ($n = 10$–20) were analysed for each individual experiment. 4,4′-BPD, a 2,2′-BPD analogue that cannot bind $Fe^{2+}$, did not induce any significant restoration of PG SK fluorescence. Error bars, s.e.m. **c**, An $ML1^{-/-}$ skin fibroblast cell showed autofluorescence in LAMP1-positive compartments. Autofluorescence (green) was detected within a range of excitation wavelengths (shown with excitation at 480 nm). No significant autofluorescence was observed for a $ML1^{+/+}$ cell. Lysosomes were stained with a LAMP1 antibody (red). Differential interference contrast (DIC) images are shown for comparison.

From the cell biology perspective, an important question to address is how TRPML channels are regulated by various cytosolic and luminal factors, and/or by proteins and lipids in the LEL membrane, especially those of which are known to be involved in endolysosomal trafficking.

## METHODS SUMMARY

**Endolysosomal electrophysiology.** HEK293T cells were either transfected with EGFP–TRPML1 alone or co-transfected with mCherry–TRPML1 and EGFP–LAMP1 (a marker for LEL). The size of the LEL is usually $<0.5\,\mu m$, which is sub-optimal for patch clamping. We therefore treated cells with 1 μM vacuolin-1 (for 1–2 h), a small chemical known to increase the size of endosomes and lysosomes selectively[23]. Large vacuoles (up to 3 μm; capacitance $= 321 \pm 101$ fF, $n = 11$) were observed in most vacuolin-treated cells (Supplementary Fig. 15). Occasionally, enlarged LEL could also been obtained from TRPML1-transfected cells without vacuolin-1 treatment. No significant difference in TRPML channel properties was seen for enlarged LEL with or without vacuolin-1 treatment. The vacuoles that were positive for both mCherry–TRPML1 and EGFP–LAMP1 were considered as enlarged LEL. Whole-lysosome, lysosome-attached and lysosome luminal-side-out recordings were performed on isolated enlarged LEL, similar to what was performed in enlarged endosomes[24]. In brief, a patch pipette (electrode) was pressed against a cell and then quickly pulled away from the cell to slice the cell membrane. Enlarged LEL were released into the dish and identified by monitoring the TRPML1–EGFP, the TRPML1–mCherry or the LAMP1–EGFP fluorescence.

**Iron quenching imaging.** HEK293T cells were loaded with 5 μM Fura-2 AM (Molecular Probes) in culture medium at 37 °C for 60 min. Cells were washed in Tyrode's solution for 10–30 min and fluorescence intensity at wavelength 360 nm ($F_{360}$) was recorded on an EasyRatioPro system (Photon Technology International). EGFP-positive cells were identified by monitoring fluorescence intensity at wavelength 470 nm ($F_{470}$). Images were analysed using ERP software.

**Full Methods** and any associated references are available in the online version of the paper at www.nature.com/nature.

**Received 26 March; accepted 1 August 2008.**
**Published online 14 September 2008.**

1. Venkatachalam, K., Hofmann, T. & Montell, C. Lysosomal localization of TRPML3 depends on TRPML2 and the mucolipidosis-associated protein TRPML1. *J. Biol. Chem.* **281,** 17517–17527 (2006).
2. Clapham, D. E. TRP channels as cellular sensors. *Nature* **426,** 517–524 (2003).
3. Nilius, B., Owsianik, G., Voets, T. & Peters, J. A. Transient receptor potential cation channels in disease. *Physiol. Rev.* **87,** 165–217 (2007).
4. Bassi, M. T. *et al.* Cloning of the gene encoding a novel integral membrane protein, mucolipidin-and identification of the two major founder mutations causing mucolipidosis type IV. *Am. J. Hum. Genet.* **67,** 1110–1120 (2000).
5. Sun, M. *et al.* Mucolipidosis type IV is caused by mutations in a gene encoding a novel transient receptor potential channel. *Hum. Mol. Genet.* **9,** 2471–2478 (2000).
6. Hentze, M. W., Muckenthaler, M. U. & Andrews, N. C. Balancing acts: molecular control of mammalian iron metabolism. *Cell* **117,** 285–297 (2004).
7. Lee, D. W., Andersen, J. K. & Kaur, D. Iron dysregulation and neurodegeneration: the molecular connection. *Mol. Interv.* **6,** 89–97 (2006).
8. Kidane, T. Z., Sauble, E. & Linder, M. C. Release of iron from ferritin requires lysosomal activity. *Am. J. Physiol. Cell Physiol.* **291,** C445–C455 (2006).
9. Gunshin, H. *et al.* Slc11a2 is required for intestinal iron absorption and erythropoiesis but dispensable in placenta and liver. *J. Clin. Invest.* **115,** 1258–1266 (2005).
10. Pryor, P. R., Reimann, F., Gribble, F. M. & Luzio, J. P. Mucolipin-1 is a lysosomal membrane protein required for intracellular lactosylceramide traffic. *Traffic* **7,** 1388–1398 (2006).
11. Xu, H., Delling, M., Li, L., Dong, X. & Clapham, D. E. Activating mutation in a mucolipin transient receptor potential channel leads to melanocyte loss in varitint-waddler mice. *Proc. Natl Acad. Sci. USA* **104,** 18321–18326 (2007).
12. Di Palma, F. *et al.* Mutations in *Mcoln3* associated with deafness and pigmentation defects in varitint-waddler (*Va*) mice. *Proc. Natl Acad. Sci. USA* **99,** 14994–14999 (2002).
13. Altarescu, G. *et al.* The neurogenetics of mucolipidosis type IV. *Neurology* **59,** 306–313 (2002).
14. Goldin, E. *et al.* Transfer of a mitochondrial DNA fragment to *MCOLN1* causes an inherited case of mucolipidosis IV. *Hum. Mutat.* **24,** 460–465 (2004).
15. Bargal, R., Goebel, H. H., Latta, E. & Bach, G. Mucolipidosis IV: novel mutation and diverse ultrastructural spectrum in the skin. *Neuropediatrics* **33,** 199–202 (2002).
16. Kress, G. J., Dineley, K. E. & Reynolds, I. J. The relationship between intracellular free iron and cell injury in cultured neurons, astrocytes, and oligodendrocytes. *J. Neurosci.* **22,** 5848–5855 (2002).
17. Petrat, F., de Groot, H. & Rauen, U. Determination of the chelatable iron pool of single intact cells by laser scanning microscopy. *Arch. Biochem. Biophys.* **376,** 74–81 (2000).
18. Goldin, E., Blanchette-Mackie, E. J., Dwyer, N. K., Pentchev, P. G. & Brady, R. O. Cultured skin fibroblasts derived from patients with mucolipidosis 4 are auto-fluorescent. *Pediatr. Res.* **37,** 687–692 (1995).
19. Kurz, T., Terman, A., Gustafsson, B. & Brunk, U. T. Lysosomes in iron metabolism, ageing and apoptosis. *Histochem. Cell Biol.* **129,** 389–406 (2008).
20. Chen, C. S., Bach, G. & Pagano, R. E. Abnormal transport along the lysosomal pathway in mucolipidosis, type IV disease. *Proc. Natl Acad. Sci. USA* **95,** 6373–6378 (1998).
21. Zeevi, D. A., Frumkin, A. & Bach, G. TRPML and lysosomal function. *Biochim. Biophys. Acta.* **1772,** 851–858 (2007).
22. Andrews, N. C. & Schmidt, P. J. Iron homeostasis. *Annu. Rev. Physiol.* **69,** 69–85 (2007).
23. Cerny, J. *et al.* The small chemical vacuolin-1 inhibits $Ca^{2+}$-dependent lysosomal exocytosis but not cell resealing. *EMBO Rep.* **5,** 883–888 (2004).
24. Saito, M., Hanson, P. I. & Schlesinger, P. Luminal chloride-dependent activation of endosome calcium channels: patch clamp study of enlarged endosomes. *J. Biol. Chem.* **282,** 27327–27333 (2007).

**Supplementary Information** is linked to the online version of the paper at www.nature.com/nature.

**Acknowledgements** This work is supported by start-up funds to H.X. from the Department of Molecular, Cellular, and Developmental Biology and Biological Science Scholar Program, University of Michigan. We thank U. Brunk, M. Saito, R. Hume, C. Duan, M. Akaaboune, J. Kuwada, S. Low, S. Punthambaker and S. Dellal for assistance, and D. Clapham, N. Andrews, L. DeFelice, L. Yue, D. Ren, C. Jiang and S. Xu for comments on an earlier version of the manuscript. We also thank K. Kiselyov for sharing his unpublished results on lysosomal iron staining of ML4 cells. We appreciate the encouragement and helpful comments from other members of the Xu laboratory.

**Author Information** Reprints and permissions information is available at www.nature.com/reprints. Correspondence and requests for materials should be addressed to H.X. (haoxingx@umich.edu).

## METHODS

**Molecular biology and biochemistry.** Full-length mouse TRPML1 and TRPML3, and a short splicing variant of mouse TRPML2 (GeneBank accession NP_001005846), were cloned into the EGFP-C2 vector (Clontech), the mCherry vector, or haemagglutinin-tag containing pcDNA3 as described previously[11]. No significant functional difference was observed among EGFP-tagged, mCherry-tagged and haemagglutinin-tagged TRPML$^{Va}$ constructs. ML4 mutants were constructed on a TRPML1$^{Va}$ background using a site-directed mutagenesis kit (Qiagen). All constructs were confirmed by sequencing analysis and protein expression was verified by western blotting. HEK293T cells were transiently transfected with wild-type TRPML1, TRPML1$^{Va}$ and ML4 mutants for electrophysiology, confocal imaging, $^{55}Fe^{2+}$ uptake and $Fe^{2+}$ quenching assays. TRPML1 western blot analyses were performed with an anti-EGFP monoclonal antibody (Covance).

**Confocal imaging.** All images were taken using a Leica (TCS SP5) confocal microscope. LAMP1 antibody was from the Iowa Hybridoma Bank and LysoTracker was from Molecular Probes (Invitrogen).

**Mammalian cell electrophysiology.** Recordings were performed in transiently transfected HEK293T cells. Cells were cultured at 37 °C, transfected using Lipofectamine 2000 (Invitrogen) and plated onto glass coverslips. No significant difference was observed for EGFP-tagged versus untagged TRPML1$^{Va}$-transfected cells. Unless otherwise stated, pipette solution contained 147 mM Cs, 120 mM methanesulphonate (MSA), 4 mM NaCl, 10 mM EGTA, 2 mM $Na_2$-ATP, 2 mM $MgCl_2$, 20 mM HEPES (pH 7.2; free $[Ca^{2+}]_i < 10$ nM). Standard extracellular bath solution (modified Tyrode's solution) contained 153 mM NaCl, 5 mM KCl, 2 mM $CaCl_2$, 1 mM $MgCl_2$, 20 mM HEPES and 10 mM glucose (pH 7.4). To reduce the background from an endogenous $Cl^-$ conductance activated by protons that was strongly outwardly rectifying[11,25], gluconate$^-$ or $MSA^-$ was used to replace most of the $Cl^-$ (remaining $[Cl^-]_o = 5$–10 mM) for all low-pH bath solutions. Low-pH 'Tyrode's' solution contained 150 mM Na-gluconate, 5 mM KCl, 2 mM $CaCl_2$, 1 mM $MgCl_2$, 10 mM glucose, 10 mM HEPES and 10 mM MES (pH 4.6). $NMDG^+$ solution contained 160 mM NMDG, 20 mM HEPES, 10 mM glucose (pH 7.4). Low-pH $NMDG^+$ solution contained 150 mM NMDG, 10 mM glucose, 10 mM MES, 10 HEPES (pH adjusted to 4.6 using MSA). 'Isotonic' metal solutions contained 105 mM metal ions, 30 mM glucose, 10 mM HEPES, 10 mM MSA and 0–30 mM $NMDG^+$ (pH 4.6). Further metal solutions (1, 3, 10 and 30 mM) were derived from mixing isotonic solutions with low-pH $NMDG^+$ solutions at various ratios. Monovalent (nominal divalent-free) solutions contained 10 mM glucose, 20 mM HEPES, 160 mM NaCl and 5 mM KCl (pH 7.4; free $Ca^{2+} < 1$–10 μM). All solutions were applied by a fast perfusion system to achieve a complete solution exchange within a few seconds. Data were collected using an Axopatch 2A patch clamp amplifier, Digidata 1440 and pClamp 10.0 software (Axon Instruments). Whole-cell currents and single channel recordings were digitized at 10 kHz and filtered at 2 kHz. Capacity current was reduced as much as possible using the amplifier circuitry. Series resistance compensation was 60%–85%. All experiments were conducted at room temperature (~21–23 °C) and all recordings were analysed with pCLAMP10 (Axon Instruments) and Origin 7.5 (Origin Lab).

**Iron de-quenching imaging.** Cultured skin fibroblast cells from a ML4 patient (*TRPML1*$^{-/-}$, clone WG0909) and corresponding heterozygous parent (*TRPML1*$^{+/-}$, clone WG0987) were obtained from the Repository for Mutant Human Cell Strains of Montreal Children's Hospital (Montreal, Canada). Fibroblast cells were loaded with 20 μM Phen Green SK (Molecular Probes) in culture medium at 37 °C for 20 min followed by a 15 min wash. Cellular fluorescence was excited at 488 nm on the PTI ERP system. Quenching of fluorescence was induced by the addition of the membrane-permeable transition metal chelator 2,2′-bipyridyl (5 mM)[17]. The 2,2′-bipyridyl analogue 4,4′-bipyridyl, which cannot bind or chelate $Fe^{2+}$, was used as a control. Because many variables such as dye loading may contribute to the variation of basal fluorescence ($F$) of PG SK, the normalized change of fluorescence ($\Delta F/F$) was used as readout to estimate the change in cytosolic $Fe^{2+}$ levels.

**Iron uptake assay.** Iron uptake was measured as described previously[25]. In brief, 30 h after transfection, HEK293T cells were washed twice with prewarmed PBS and then incubated with 1 ml of prewarmed uptake assay buffer (25 mM Tris, 25 mM MES, 140 mM NaCl, 5.4 mM KCl, 5 mM glucose, 1.8 mM $CaCl_2$, 800 μM MgSO4, 50 μM ascorbic acid, pH 5.8) containing $^{55}$Fe-nitrilotriacetic acid (NTA, 1 μM $^{55}$Fe) at 37 °C for 5 min. $^{55}$Fe-NTA was made by mixing $^{55}FeCl_3$ (PerkinElmer) with 100 mM NTA in a 1:50 molar ratio. Ascorbic acid (100 mM) was used to promote the formation and maintenance of ferrous ($Fe^{2+}$) iron (adjusted to pH 5.8). All uptake assays were performed with 20 μM $Fe^{2+}$ (with a 1:20 molar ratio for $^{55}FeCl_3$ and $FeSO_4$) at pH 5.8. Assays were stopped by the addition of 2 ml ice-cold PBS. After washing three times with ice-cold PBS, the cells were detached and collected by adding 1 ml 0.25% trypsin-EDTA. Parallel experiments were conducted at 0 °C to measure the cell surface $^{55}$Fe binding, which was subtracted from the values at 37 °C to obtain the net iron uptake. Cell-associated radioactivity was measured with liquid scintillation spectrometry.

**Lysosomal iron staining.** Lysosome iron was stained using a modified sulphide-silver method[19]. In brief, fibroblast cells were grown on coverslips and exposed to 50 μM $Fe^{3+}$-dextran overnight. Cells were then washed with PBS and fixed with 2% glutaraldehyde in 0.1 M Na-cacodylate buffer with 0.1 M sucrose (pH 7.2) for 1.5 h at room temperature (22 °C). Next cells were sulphidated at ~pH 9 with 1% (w/v) ammonium sulphide in 70% (v/v) ethanol for 15 min. The development was then performed using a physical, colloid-protected developer containing silver-lactate and hydroquinone for 1–2 h.

**Reagents.** 2,2'-BPD, 4,4'-BPD, iron ascorbate, ferric chloride, iron dextran, and all other metal salts were from Sigma Chemicals.

**Data analysis.** Most data are presented as the mean ± s.e.m. Statistical comparisons were made using analysis of variance (ANOVA). A $P$ value $< 0.05$ was considered statistically significant.

25. Xu, H., Jin, J., DeFelice, L. J., Andrews, N. C. & Clapham, D. E. A spontaneous, recurrent mutation in divalent metal transporter-1 exposes a calcium entry pathway. *PLoS Biol.* **2**, E50 (2004).

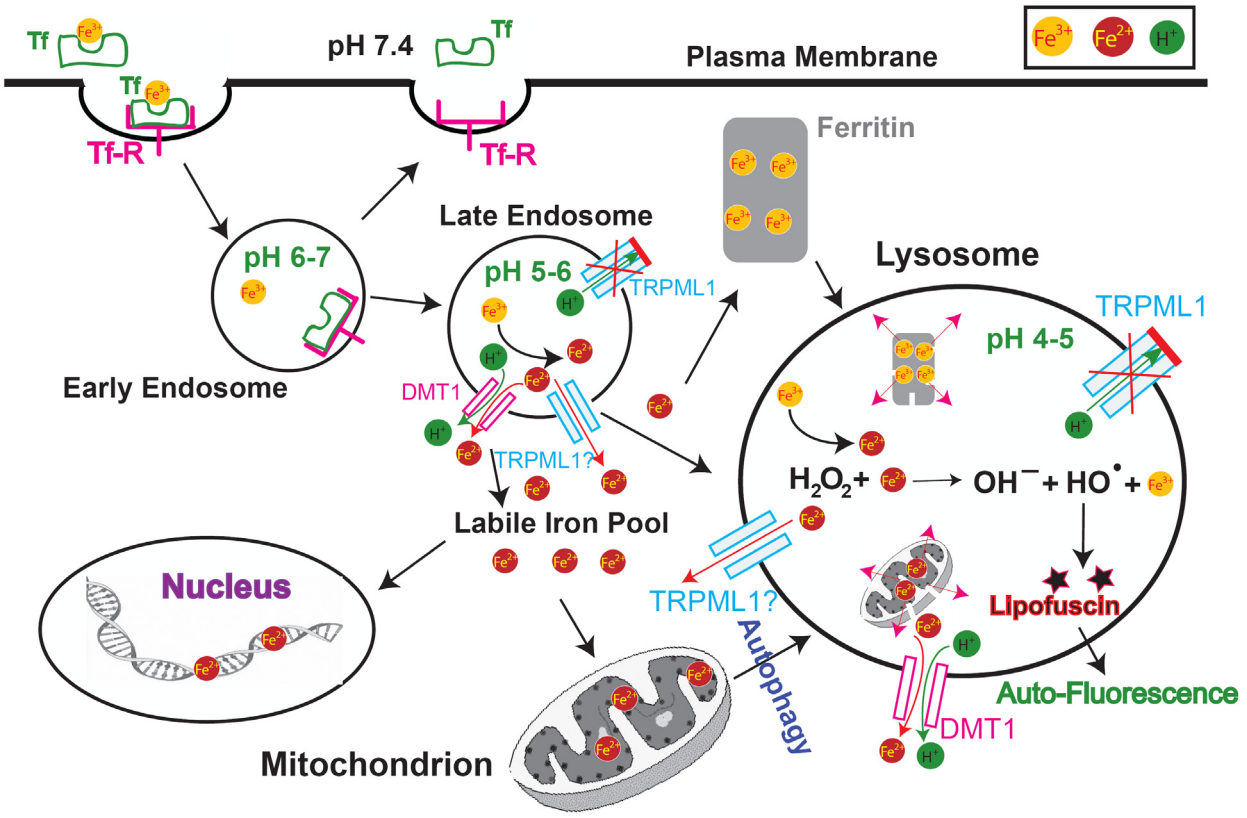


**Supplementary Figure 1. Intracellular iron metabolism pathways.**

In most mammalian cells, the uptake of iron is initiated by the binding of circulating $Fe^{3+}$ to transferrin (Tf), an abundant protein with an extraordinarily high affinity for $Fe^{3+}$. Binding of Tf to its receptor (transferrin receptor, Tf-R) results in endocytosis of the whole complex. The acidic environment of endosomes can trigger a release of $Fe^{3+}$ from the Tf/Tf-R complex, allowing it to recycle back to the plasma membrane for reuse. A ferrireductase reduces $Fe^{3+}$ to $Fe^{2+}$, and $Fe^{2+}$ is then released into the cytoplasm via the Divalent metal transporter 1 (DMT1) in an $H^+$-dependent manner. DMT1 is highly expressed in developing erythroid precursors, as well as in endosomes and lysosomes of some other, but not all cell types. Because Tf-R is ubiquitously expressed, it is hypothesized that a DMT1-independent iron transport protein is present in endosomes and lysosomes of most cell types. We propose that TRPML1 participates in an $Fe^{2+}$-release mechanism. Released $Fe^{2+}$ constitutes the free/chelatable iron pool (also called labile iron pool) of the cell, which provides Fe cofactors required for many essential

enzymes such as the mitochondrial electron-transport complexes. The remaining Fe that is not bound by enzymes, is converted into $Fe^{3+}$ and stored by the multimeric protein ferritin. To restore $Fe^{2+}$ pools when needed, lysosomal degradation produces redox-active $Fe^{2+}$ for release into the cytoplasm. Lysosomal degradation also performs iron recycling of many other iron-containing proteins such as metalthioneins. During oxidative stress, lysosomal redox-active $Fe^{2+}$ catalyze the production of extremely reactive hydroxyl radicals ($OH^{\bullet}$; Fenton reaction) which oxidize lysosomal contents (proteins, lipids, and carbohydrates), and in the presence of $Fe^{2+}$, can result in non-degradable, auto-fluorescent substances called lipofuscin. Lipofuscin usually accumulates only in aged post-mitotic cells such as muscles and neurons and therefore is often referred to as an "aging pigment".

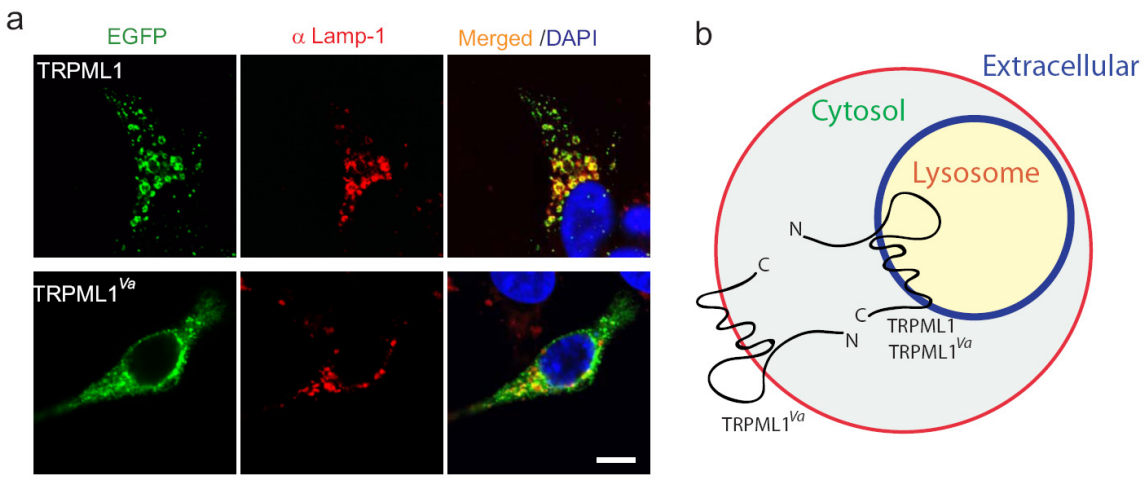


**Supplementary Figure 2. Subcellular localizations of wt TRPML1 and TRPML1$^{Va}$ proteins.**

**a)** Confocal images of fixed HEK293T cells that were transfected with EGFP-TRPML1 and EGFP-TRPML1$^{Va}$. Cells were immunostained using Lamp1 antibody and loaded with DAPI. EGFP-TRPML1 was primarily localized in Lamp1-positive compartments. TRPML1$^{Va}$ however, were localized throughout the cell including Lamp1-positive compartments. **b)** A cartoon illustrating the putative membrane topology of TRPML1 or TRPML1$^{Va}$ at the plasma membrane and the membranes of late endosomes and lysosomes. Both N- and C- termini of TRPML1 are predicted to be on the cytosolic side when the channel is located either at the cell surface (plasma membrane) or in the late endosome/lysosome.

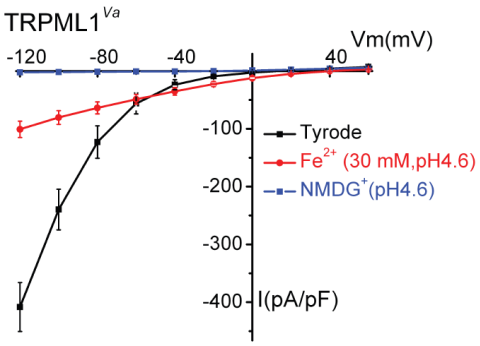


**Supplementary Figure 3. TRPML1$^{Va}$-mediated currents in different bath solutions.** Average I-V relations of currents (n = 5 cells) induced by Tyrode's ($I_{TRPML1\text{-}Va}$), $Fe^{2+}$ (30 mM, pH 4.6; $I^{Fe}_{TRPML1\text{-}Va}$), and $NMDG^{+}$ (pH 4.6) solutions.

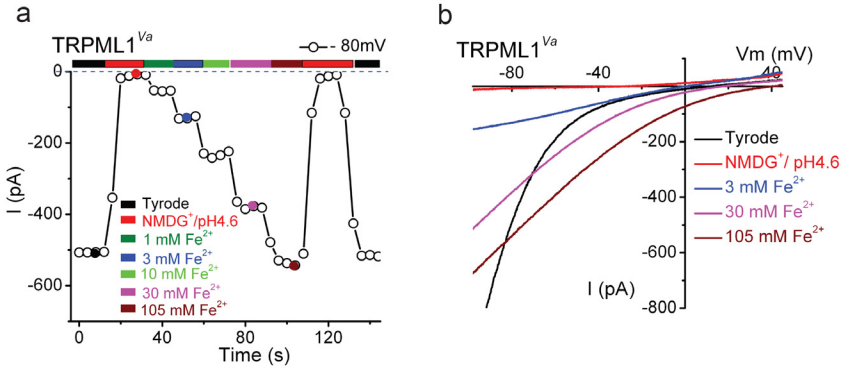


**Supplementary Figure 4. $[Fe^{2+}]_o$- dependence of $I^{Fe}_{TRPML1\text{-}Va}$.**

**a)** $I^{Fe}_{TRPML1\text{-}Va}$ induced by various concentrations (0, 1, 3, 10, 30, and 105 mM) of $Fe^{2+}$ (pH 4.6) versus Tyrode's solution and $NMDG^{+}$ solution at -80 mV. Significant inward $I^{Fe}_{TRPML1\text{-}Va}$ was seen at 1 mM- $[Fe^{2+}]_o$ with an average current density of 11.7 ± 1.7 pA/pF at -80 mV (n = 10). At -80 mV, $[Fe^{2+}]_o$ required for half maximal current was 5.2 ± 1 mM with a hill slope of 1.4 ± 0.3 (n = 9). **b)** Representative whole-cell $I^{Fe}_{TRPML1\text{-}Va}$ currents. In response to increased $[Fe^{2+}]_o$ , the reversal potential of $I^{Fe}_{TRPML1\text{-}Va}$ was shifted toward a more positive potential, consistent with the conclusion that $Fe^{2+}$ is the charge carrier for $I^{Fe}_{TRPML1\text{-}Va}$.

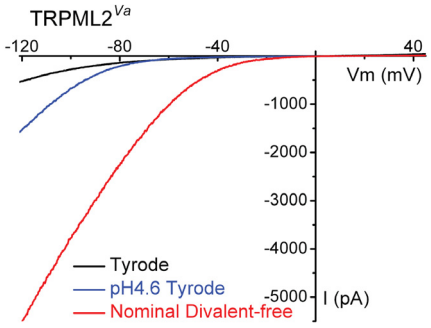


**Supplementary Figure 5. A TRPML2$^{Va}$-expressing HEK293T cell displayed a pH-sensitive inwardly rectifying current.**

Whole-cell currents were elicited by a ramp protocol from -140 mV to +140 mV. Lowering the extracellular pH (to pH 4.6) of the bath solution (Tyrode's) significantly

increased the inward current in this TRPML2$^{Va}$-expressing cell. A much larger inward current was induced by Nominal Divalent-free Tyrode solution in the same cell.

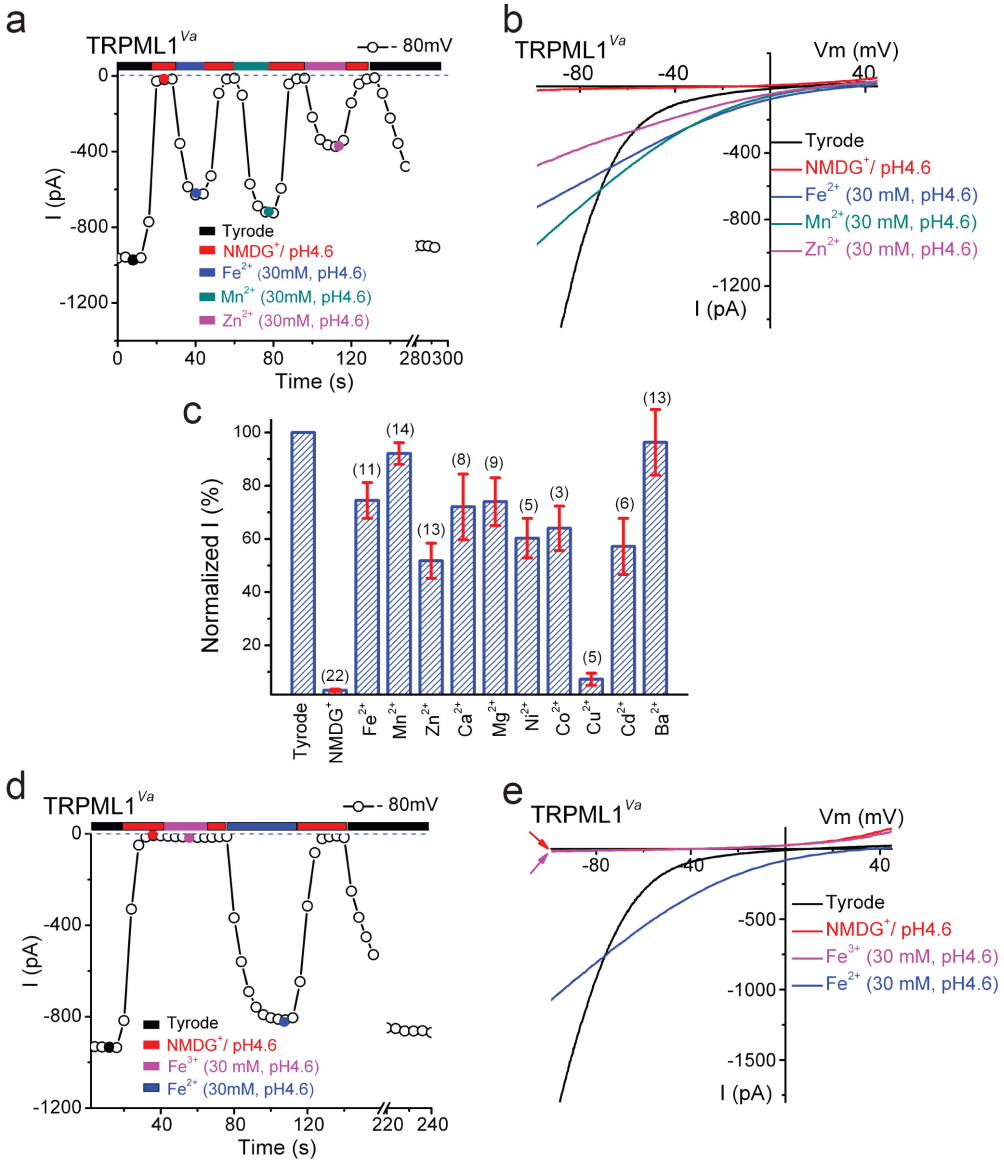


**Supplementary Figure 6. TRPML1 is permeable to most divalent trace metals, but not ferric.**

**a, b)** $I_{TRPML1\text{-}Va}$ elicited by extracellular $Fe^{2+}$, $Mn^{2+}$, and $Zn^{2+}$ solutions (30 mM, pH 4.6). In the presence of $Mn^{2+}$ and $Zn^{2+}$, large inward currents were evoked (pH 4.6). **c)** Current densities (mean ± SEM, n = 3-14) of $I_{TRPML1\text{-}Va}$ induced by various metal solutions measured at -80 mV

and normalized by cell capacitance. At -80 mV, the currents for $Fe^{2+}$, $Mn^{2+}$, and $Zn^{2+}$ were 74 ± 8.6 pA/pF (n = 24), 80 ± 15 pA/pF (n = 14), and 54 ± 13 pA/pF (n = 13), respectively. The overall sequence of divalent permeability determined in our assays is: $Ba^{2+}>Mn^{2+}>Fe^{2+}\sim Ca^{2+}\sim Mg^{2+}>Ni^{2+}\sim Co^{2+}\sim Cd^{2+}>Zn^{2+}>>Cu^{2+}$ (pH 4.6). **d, e)** No significant inward current (1.3 ± 0.5 pA/pF at -80 mV, n = 6) was evoked by 30 mM $Fe^{3+}$ (pH 4.6) in TRPML1$^{Va}$-expressing cells, in contrast to large $Fe^{2+}$ currents detected in the same cells.

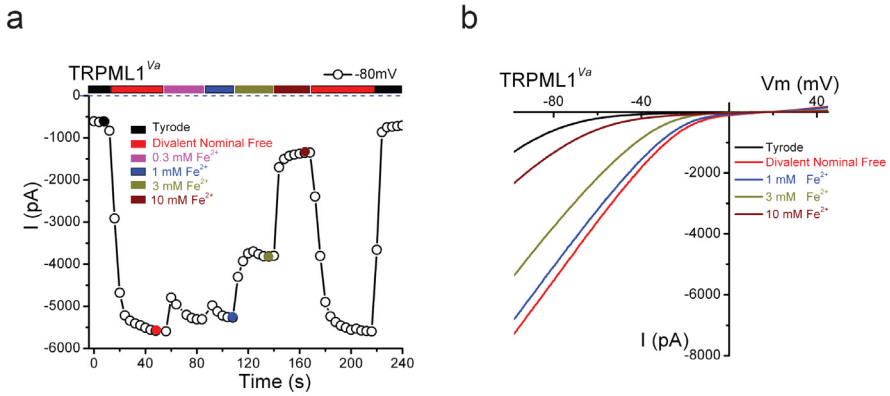


**Supplementary Figure 7. $[Fe^{2+}]_o$- dependent inhibition of monovalent $I_{TRPML1\text{-}Va}$.** **a)** TRPML1$^{Va}$ displays large monovalent currents in the absence of divalent cations. Monovalent $I_{TRPML1\text{-}Va}$ was inhibited by $Ca^{2+}$ (data not shown), suggesting that $Ca^{2+}$ and $Na^{+}$ permeate through TRPML1 via a common conduction pathway. Similarly, addition of 1-10 mM $Fe^{2+}$ dose-dependently inhibited the $Na^{+}$ $I_{TRPML1\text{-}Va}$, suggesting that $Fe^{2+}$ may permeate through TRPML1 in the same conduction pathway as $Na^{+}$ and $Ca^{2+}$. **b)** Representative I-V relations of currents at various concentrations of $Fe^{2+}$ shown in (**a**).

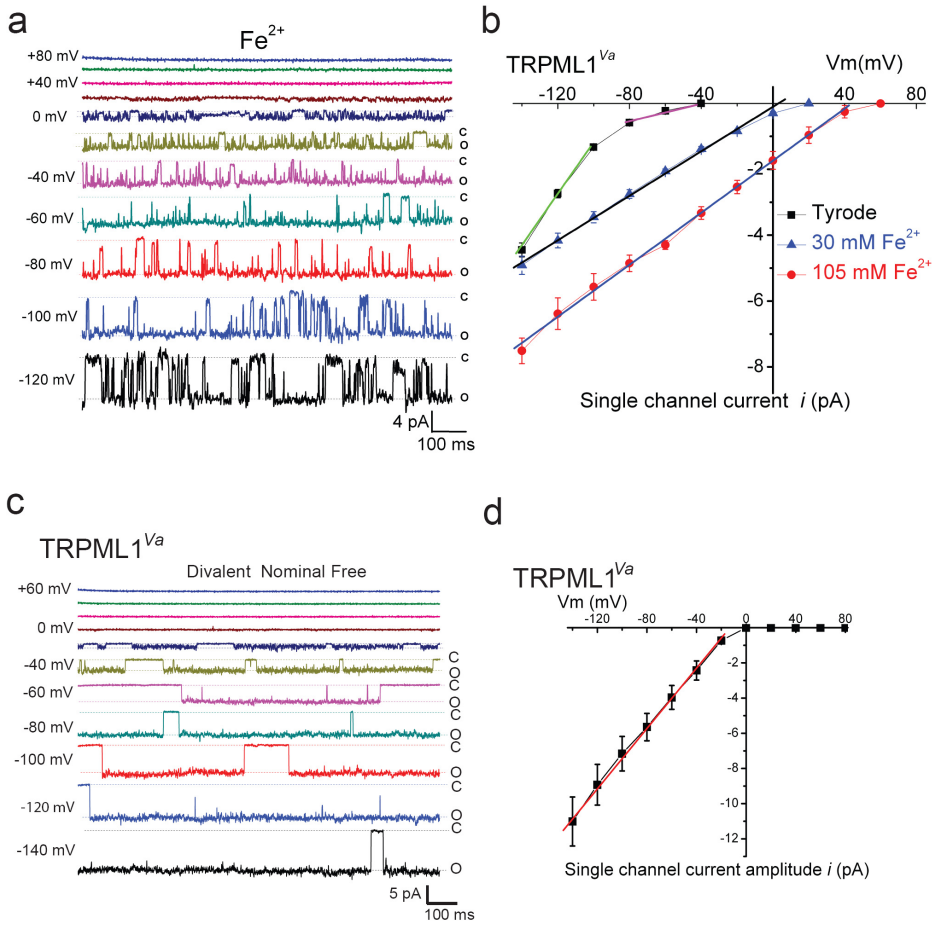


**Supplementary Figure 8. Single channel properties of TRPML1.**

**a)** Single channel $i^{Fe}_{TRPML1\text{-}Va}$ in an inside-out patch. The pipette solution contained isotonic $Fe^{2+}$ (105 mM, pH 4.6) solution, while the bath solution contained a $Cs^{+}$-based internal solution (147 mM Cs-Mes). Downward deflection indicates channel openings at negative potentials. "C" and "O" indicate closed and open levels, respectively. The mean open and closed times at -120 mV were 36 ± 2.6 ms and 2 ± 0.8 ms, respectively. **b)** Single channel conductance of $i^{Fe}_{TRPML1\text{-}Va}$ (30 mM and 105 mM $Fe^{2+}$). The conductance was 40 ± 3 pS (n = 7; from -140 mV to + 40 mV) for 105 mM $Fe^{2+}$, and 32 ± 1 pS (n = 4; from -140 mV to 0 mV) for 30 mM $Fe^{2+}$, respectively. For comparison, single $i_{TRPML1\text{-}Va}$ conductance was 75 ± 5 pS (n = 9) from -140 mV to -100 mV, and 12 ± 0.4 (n = 9) from -80 mV to -40 mV, respectively. **c)** Single monovalent $i_{TRPML1\text{-}Va}$. The pipette solution contained Nominal Divalent-free Tyrode solution (free $Ca^{2+}$ ~ 1-10 μM), which resulted in kinetics different from $i^{Fe}_{TRPML1\text{-}Va}$. **d)** Single monovalent $i_{TRPML1\text{-}Va}$ conductance was 83 ± 6 pS (n = 7) from -140 mV to - 20 mV.

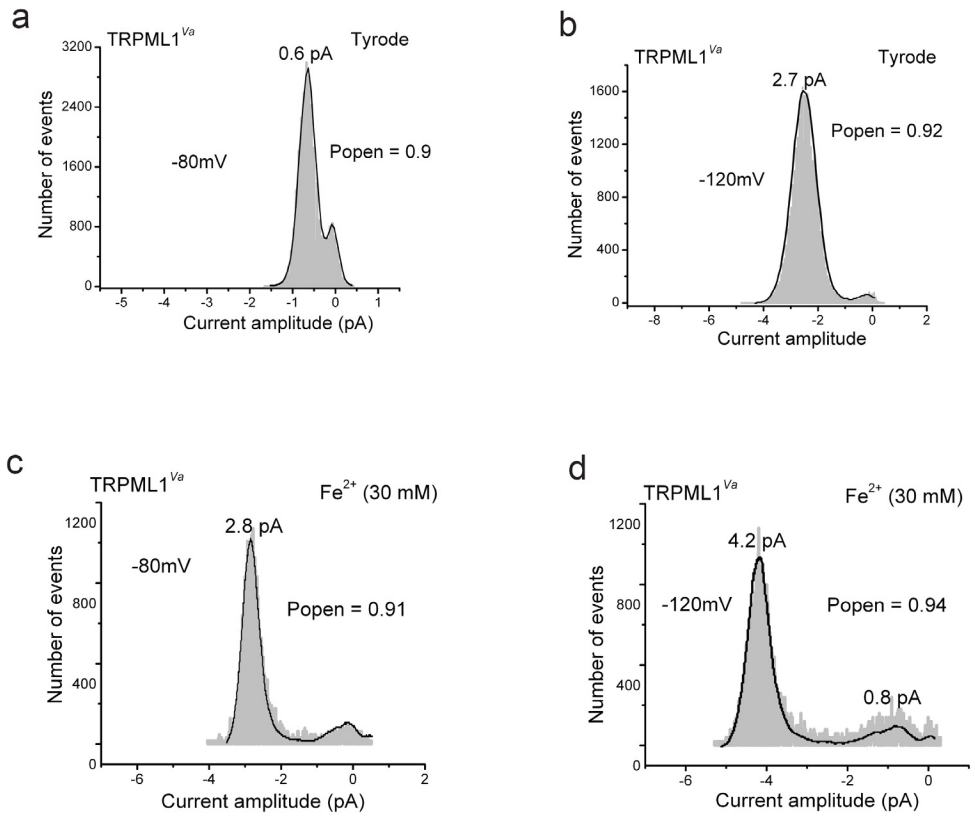


**Supplementary Figure 9. Analysis of single-channel TRPML1$^{Va}$ currents.**

**a)** Histograms of single $i_{\text{TRPML1- Va}}$ channel openings at -80 mV. **b)** Histogram analysis of single $i_{\text{TRPML1- Va}}$ channel openings at -120 mV. **c)** Histogram analysis of single $i^{Fe}{}_{\text{TRPML1- Va}}$ channel openings at -80 mV. **d)** Histogram analysis of single $i^{Fe}{}_{\text{TRPML1- Va}}$ channel openings at -120 mV.

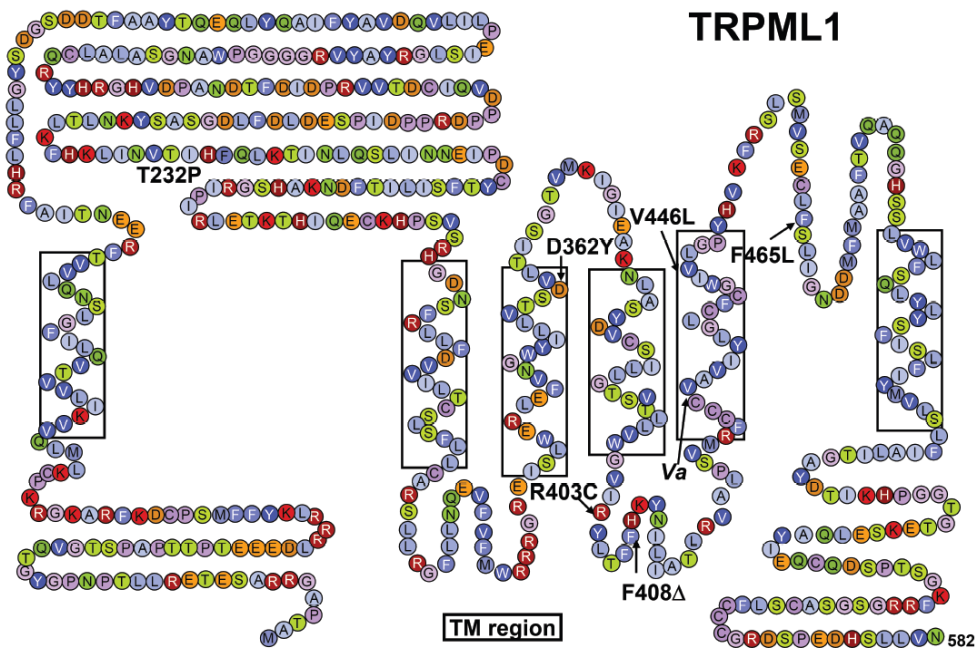


**Supplementary Figure 10. TRPML1 membrane topology and ML4 mutations studied in this work**.

ML4 patients carrying the following mis-sense mutations are compound heterozygous: T232P, D362Y, R403C, F408Δ, V446L, and F465L. The other allele contains "major" or "minor" mutations, both of which are large deletions of the TRPML1 gene and are expected to be null. All ML4 mutations (studied in the current work) were introduced into the background of TRPML1$^{Va}$.

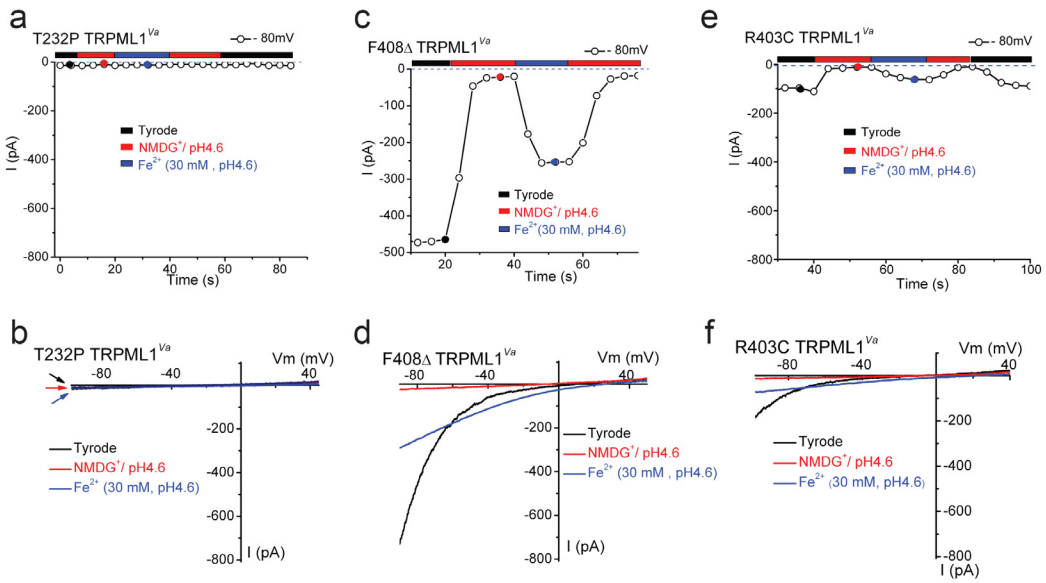


**Supplementary Figure 11. $Fe^{2+}$ permeability of the TRPML1 channel is impaired by ML4 mutations.**

**a, b)** Lack of $I^{Fe}$ in a cell expressing T232P-TRPML1$^{Va}$ channel. **c, d)** $I^{Fe}$ of F408Δ-TRPML1$^{Va}$ channel. **e. f)** $I^{Fe}$ of R403C-TRPML1$^{Va}$ channel.

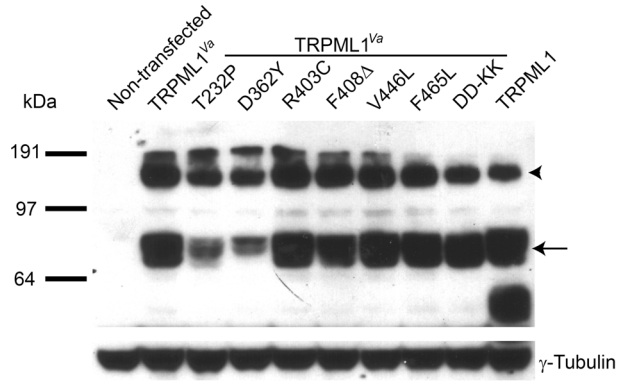


**Supplementary Figure 12. Protein expression levels of wt and mutant TRPML1 proteins.**

Cell lysates were prepared from HEK293T cells transfected with EGFP-TRPML1, EGFP-TRPML1$^{Va}$, and various ML4 mutant EGFP-TRPML1$^{Va}$ channels. The Western blot was probed with an anti- EGFP antibody. The arrow indicates the ~ 75-kDa band of EGFP-TRPML1 or other EGFP-TRPML1-derived mutant proteins. Arrow head indicates a band of ~ 150 kDa, probably resulting from a dimer of EGFP-TRPML1 or its mutants. A smaller ~ 35 kDa band was only seen in wt TRPML1-transfected cells. The lower panels show the loading controls probed by anti–γ tubulin.

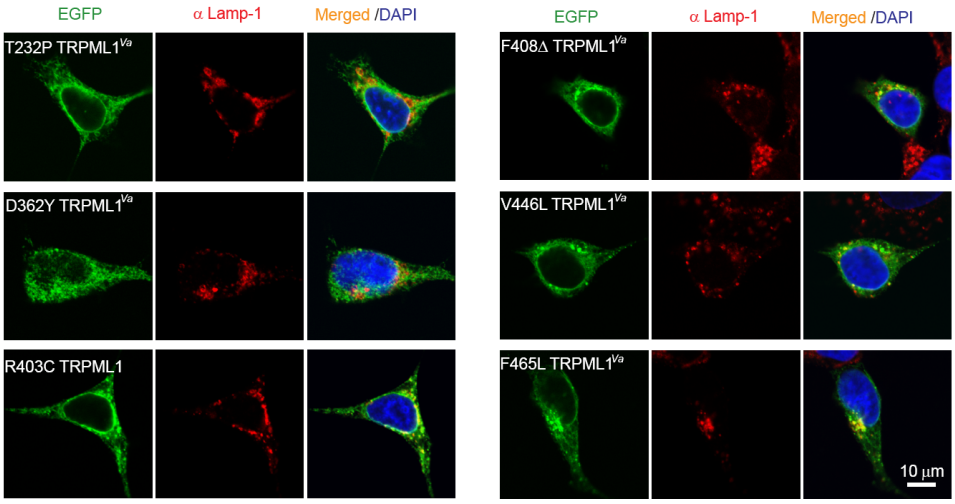


**Supplementary Figure 13. Subcellular localizations of ML4 mutant TRPML1$^{Va}$ proteins.** Confocal images of fixed HEK293T cells that were transfected with various ML4 mutant EGFP-TRPML1$^{Va}$ channels. All cells were immunostained using Lamp1 antibody and loaded with DAPI. Similar to TRPML1$^{Va}$, ML4 mutant TRPML1$^{Va}$ proteins were localized throughout the cell including Lamp1 positive compartments.

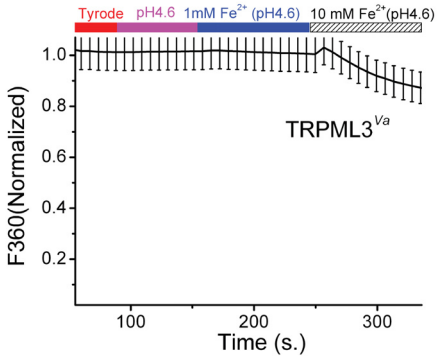


**Supplementary Figure 14. $Fe^{2+}$-mediated fluorescence quenching in TRPML3$^{Va}$-transfected cells.** While no significant quenching was seen at 1 mM $Fe^{2+}$, a very slow rate of quenching was observed at 10 mM $Fe^{2+}$. The expression of TRPML3$^{Va}$ was confirmed by measuring EGFP fluorescence at an excitation wavelength of 470 nm (F470). Fura-2 fluorescence was detected using an excitation wavelength of 360 nm (F360).

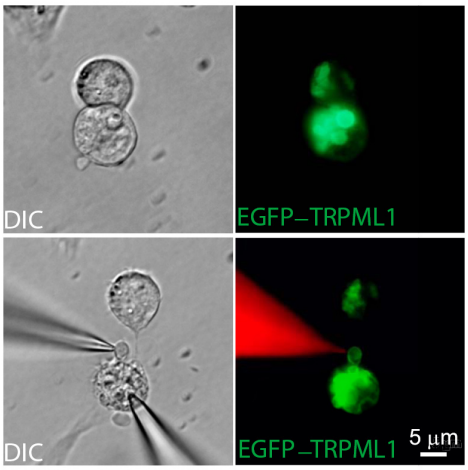


**Supplementary Figure 15. Isolation of single enlarged lysosomes from HEK293T cells.** *Top panels* show two EGFP-TRPML1-expressing HEK293T cells that were pre-treated with vacuolin-1. The large EGFP-positive vacuoles were enlarged LE/Ly based on Lamp-1 immunoreactivity or LysoTracker staining (not shown). In the *lower panels*, a patch pipette (pulling pipette, the lower one) was pressed against the lower cell and then quickly pulled away from the cell to slice the cell membrane. Enlarged LE/Ly was released into the dish. Recordings were made on a TRPML1 –positive enlarged lysosome using a recording pipette (filled with Rhodamine B dye for the purpose of illustration).

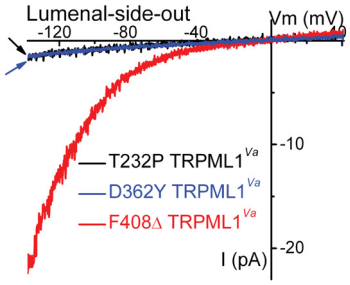


**Supplementary Figure 16. ML4 mutations impair the channel activity of TRPML1 in the lysosome.**

$I_{Tyrode}$ of T232P-, D362Y-, and F408Δ-TRPML1$^{Va}$ from Lumenal-side-out patches.

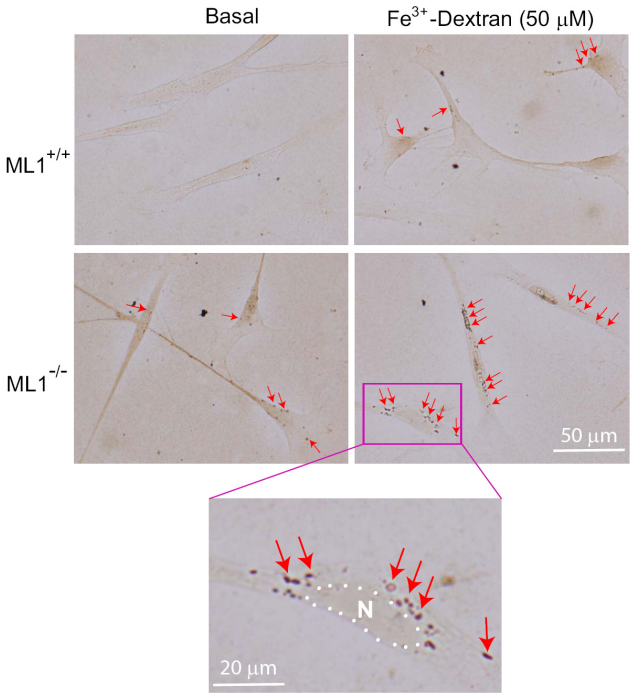


**Supplementary Figure 17. TRPML1-deficient cells exhibit increased intra-lysosomal iron levels.**

Lysosomal iron was stained in cultured human skin fibroblast cells using the sulphide-silver method (*SSM*). Both cultured TRPML1$^{-/-}$ (ML1$^{-/-}$) and control (ML1$^{+/+}$) fibroblasts were loaded with $Fe^{3+}$-dextran (50 μM) overnight. Under this condition, endocytosed iron is expected to be localized exclusively in the lysosomes. In comparison to cells without treatment of $Fe^{3+}$-dextran (basal), $Fe^{3+}$-dextran treated cells (both ML1$^{-/-}$ and ML1$^{+/+}$) exhibited significantly more iron staining (shown with red arrows). Significantly more lysosomal iron staining was seen in ML1$^{-/-}$ fibroblasts than in ML1$^{+/+}$ cells. Sparse iron staining was seen in ML1$^{-/-}$, but not ML1$^{+/+}$ cells. The bottom panel shows an enlarged view of lysosomal iron staining from $Fe^{3+}$-treated ML1$^{-/-}$ cells. Most lysosomal iron staining was in the vicinity of the nucleus (N; dotted line).

## Supplementary Discussion

Trace metal ions such as $Fe^{2+}$, $Mn^{2+}$, $Cu^{2+}$, $Zn^{2+}$, and $Co^{2+}$ are required cofactors for many essential cellular enzymes, yet the mechanisms for metal ion uptake in mammalian cells are not fully understood. The primary pathway for cellular iron uptake depends on receptor-mediated endocytosis of $Fe^{3+}$-bound transferrin, reduction of $Fe^{3+}$ to $Fe^{2+}$, and the subsequent release/exit of $Fe^{2+}$ from late endosomes into the cytosol (**Supplementary Fig. 1)** [1]. However, most cytosolic $Fe^{2+}$ is released following lysosomal degradation of ferritin-Fe complexes and autophagic ingestion of iron-containing macromolecules [1,2]. The principal mechanism responsible for transporting $Fe^{2+}$ from the lumen of the late endosome and lysosome (LE/Ly) into the cytosol, nevertheless, has remained elusive [3,4]. DMT1, the only protein currently known to mediate cellular iron uptake in mammalian cells, is highly expressed in developing erythroid precursors, as well as in endosomes and lysosomes of some other, but not all cell types [3,5]. TRPML1 is ubiquitously expressed (in cells of every tissue) [6] and primarily localized in the LE/Ly [7,8]. Mucolipidosis type IV (ML4) patients exhibit iron-deficiency anemia [6,9], which is believed to result from reduced gastric acid secretion in these patients [10]. Vitamin B12 breakdown and absorption during digestion is known to be strongly dependent on stomach acid levels [11], and yet ML4 patients do not exhibit Vitamin B12 deficiency [9,10], a symptom associated with most *hypochlorhydric* states [12]. One explanation for these findings is that there may be a direct link between TRPML1 expression and iron uptake.

In this paper we have demonstrated that TRPML1 plays a critical role in cellular iron homeostasis. Our principal result is that the degree of the impaired $Fe^{2+}$ permeability exhibited by ML4 mutations correlates well with disease severity observed in ML4 patients, whether these channels are mis-expressed on the plasma membrane or are studied in their native endo-

lysosomal membranes. To support our conclusion, we obtained additional data using iron imaging and iron staining approaches to show the cytosolic $Fe^{2+}$ deficiency with concurrent intra-lysosomal iron overload in ML4 cells. Because all the mutations we have studied so far also alter $Ca^{2+}$ permeation through the channels, it remains a formal possibility that an alteration in $Ca^{2+}$ flux through the channel might act on iron homeostasis through indirect pathways such as affecting the trafficking/endocytosis. ML4 cells exhibit a defect in the late endocytic pathway [8,13-15], suggesting that $Ca^{2+}$ permeability of TRPML1 may be required for $Ca^{2+}$-dependent fusion/fission of LE/Ly. However, this defect in vesicular transport cannot explain the cytosolic $Fe^{2+}$ deficiency that we observed since the internalization and recycling of the transferrin receptor is normal in ML4 cells [13], and lysosomal $Fe^{2+}$ release (into the cytosol) is most likely to be mediated directly by an iron-conducting channel/transporter, as is the case for DMT1[16]. Therefore, by far the simplest explanation of our results is that the $Fe^{2+}$ release pathway between the cytosol and the lysosome lumen is blocked/inactivated in cells with ML4 mutations. Thus we conclude that TRPML1 is likely serving as an essential iron release channel from the late endosome/lysosome. While a ML4-induced- loss of $Ca^{2+}$ permeability may result in a defect of lysosomal trafficking or exocytosis [15,17] and subsequent accumulation of various lipids in LE/Ly, the degradation of these materials is normal [13,15]. Therefore, these accumulated substances would become most harmful only if they are oxidized to generate lipofuscin-like non-degradable materials in the presence of high intra-lysosomal $Fe^{2+}$ [4]. It remains unknown whether and how these lipofuscin-like materials contribute to the retinal- and neural- degenerative symptoms of ML4 patients. Nevertheless, lipofuscin-like molecules preferentially accumulate in post-mitotic cells such as muscle cells and neurons, which are primarily affected in ML4 patients [15].

Although enlargement of LE/Ly in ML4 cells may result from a defect in $Ca^{2+}$-dependent lysosome maturation and reformation [18], our results suggest that the impaired metabolism of iron and other heavy metals may also been involved. Indeed, increased levels of lysosomal $Fe^{2+}$ resulting from iron overload is reported to induce an enlargement of lysosomes [19]. Interestingly, the lysosomal phenotype of the *cup-5* null mutant, which is *C. elegans* ortholog of human TRPML1, can be suppressed by inactivating MRP-4 [20], a member of the ABC transporter superfamily known to be required for heavy metal resistance in *C. elegans* [21]. Another consideration is whether TRPML1 channels have a role in $Fe^{2+}$ transport at the plasma membrane in special cell types. For example, the expression of TRPML1 in the lung and intestine [22] combined with TRPML1's verapamil-sensitivity [23], suggest that TRPML1 (or TRPML2) may play a role in pulmonary verapamil-sensitive $Mn^{2+}$ uptake [24] and intestinal iron absorption. Although a preliminary study failed to reveal systemic iron deficiency in TRPML1 KO mice [25], human ML4 patients do exhibit systemic iron deficiency and/or anemia [9,10]. These results, together with our findings that ML4 cells display cellular iron deficiency, suggests that genetic and functional compensation may occur at whole-animal level, which is commonly observed for iron-related mouse studies [16,26]. Nevertheless, the essential role of TRPML1 in cellular iron metabolism suggests that lysosome-targeting iron chelators might alleviate the degenerative symptoms of ML4 patients**.** From the cell biology perspective, a key question to ask is how TRPML channels are regulated by various cytosolic and lumenal factors, and/or by proteins and lipids in the LE/Ly membrane, especially those of which are known to be involved in endo-lysosomal trafficking.

## Supplementary References


1 M. W. Hentze, M. U. Muckenthaler, and N. C. Andrews, *Cell* **117** (3), 285 (2004).
2 T. Z. Kidane, E. Sauble, and M. C. Linder, *Am J Physiol Cell Physiol* **291** (3), C445 (2006).
3 H. Gunshin, Y. Fujiwara, A. O. Custodio et al., *The Journal of clinical investigation* **115** (5), 1258 (2005).
4 T. Kurz, A. Terman, B. Gustafsson et al., *Histochemistry and cell biology* **129** (4), 389 (2008).
5 H. Gunshin, B. Mackenzie, U. V. Berger et al., *Nature* **388** (6641), 482 (1997); H. Xu, J. Jin, L. J. DeFelice et al., *PLoS biology* **2** (3), E50 (2004).
6 M. Sun, E. Goldin, S. Stahl et al., *Human molecular genetics* **9** (17), 2471 (2000).
7 B. Nilius, G. Owsianik, T. Voets et al., *Physiological reviews* **87** (1), 165 (2007); K. Venkatachalam, T. Hofmann, and C. Montell, *The Journal of biological chemistry* **281** (25), 17517 (2006).
8 P. R. Pryor, F. Reimann, F. M. Gribble et al., *Traffic (Copenhagen, Denmark)* **7** (10), 1388 (2006).
9 G. Altarescu, M. Sun, D. F. Moore et al., *Neurology* **59** (3), 306 (2002).
10 R. Schiffmann, N. K. Dwyer, I. A. Lubensky et al., *Proceedings of the National Academy of Sciences of the United States of America* **95** (3), 1207 (1998).
11 G. S. Bradford and C. T. Taylor, *The Annals of pharmacotherapy* **33** (5), 641 (1999).
12 I. L. Salom, S. E. Silvis, and A. Doscherholmen, *Scandinavian journal of gastroenterology* **17** (1), 129 (1982).
13 C. S. Chen, G. Bach, and R. E. Pagano, *Proceedings of the National Academy of Sciences of the United States of America* **95** (11), 6373 (1998).
14 J. P. Luzio, N. A. Bright, and P. R. Pryor, *Biochemical Society transactions* **35** (Pt 5), 1088 (2007).
15 D. A. Zeevi, A. Frumkin, and G. Bach, *Biochim Biophys Acta* (2007).
16 N. C. Andrews and P. J. Schmidt, *Annual review of physiology* **69**, 69 (2007).
17 J. P. Luzio, B. A. Rous, N. A. Bright et al., *Journal of cell science* **113 ( Pt 9)**, 1515 (2000); J. M. LaPlante, M. Sun, J. Falardeau et al., *Molecular genetics and metabolism* **89** (4), 339 (2006); J. P. Luzio, P. R. Pryor, and N. A. Bright, *Nature reviews* **8** (8), 622 (2007).
18 H. Fares and I. Greenwald, *Nature genetics* **28** (1), 64 (2001).
19 B. M. Myers, F. G. Prendergast, R. Holman et al., *The Journal of clinical investigation* **88** (4), 1207 (1991).
20 L. Schaheen, G. Patton, and H. Fares, *Development (Cambridge, England)* **133** (19), 3939 (2006).
21 A. Broeks, B. Gerrard, R. Allikmets et al., *The EMBO journal* **15** (22), 6132 (1996).
22 M. T. Bassi, M. Manzoni, E. Monti et al., *American journal of human genetics* **67** (5), 1110 (2000).
23 H. Xu, M. Delling, L. Li et al., *Proceedings of the National Academy of Sciences of the United States of America* **104** (46), 18321 (2007).

24 E. A. Heilig, K. J. Thompson, R. M. Molina et al., *American journal of physiology* **290** (6), L1247 (2006).
25 B. Venugopal, M. F. Browning, C. Curcio-Morelli et al., *American journal of human genetics* **81** (5), 1070 (2007).
26 F. Canonne-Hergaux, S. Gruenheid, P. Ponka et al., *Blood* **93** (12), 4406 (1999).